OPTICAL INVESTIGATIONS OF ULTRA-SMALL COLLOIDAL NANOPARTICLES AND HETERONANOPARTICLES BASED ON II–VI SEMICONDUCTORS

M.YA. VALAKH,[1] V.M. DZHAGAN,[1] A.E. RAEVSKAYA,[2] S.YA. KUCHMIY[2]

[1]V. Lashkaryov Institute of Semiconductor Physics, Nat. Acad. of Sci. of Ukraine
(41, Prosp. Nauky, Kyiv 03028, Ukraine; e-mail: dzhagan@isp.kiev.ua)

[2]Institute of Physical Chemistry, Nat. Acad. of Sci. of Ukraine
(31, Prosp. Nauky, Kyiv 03028, Ukraine)

Colloidal II–VI semiconductor nanoparticles (NPs) and core–shell NPs obtained by means of colloidal chemistry are studied by means of optical absorption, photoluminescence, and Raman scattering spectroscopy. The effects of the strong confinement of charge carriers and lattice vibrations in small (< 3 nm) NPs are considered. The influence of the passivating shell onto the electronic bandgap, photoluminescence spectrum, and phonon spectrum is established. The drastic differences in resonant Raman spectra of ultra-small (< 2 nm) nanoparticles are found, which are related to the strong spatial localization of vibrations, as well as to the structural rearrangement due to the surface effect.

1. Introduction

For the past decade, II–VI semiconductor nanoparticles (NPs) have become an object of particular research interest due to their unique size-dependent optical properties that have already found numerous applications [1–15]. A number of techniques have been elaborated to obtain II-VI nanoparticles of various sizes and topologies to tailor the expected physical characteristics, especially luminescence, whose spectral position can be effectively varied across a broad range [1, 2, 6], the methods of colloidal synthesis being the most appropriate for the fabrication of nanoparticles with good optical quality and small size dispersion. Nanoparticles of cadmium chalcogenides and composite core/shell nanostructures based on them have been extensively studied, e.g. as photocatalysts, as potential active media for optical and optoelectronic devices, solar cells, memory elements, as fluorescent labels in biophysical experiments and other applications [6–10, 16–18]. Hence, the interest in the growth and the characterization of these NPs, as well as in their extended optical studies, is driven by both fundamental and applied aspects.

Here, we report on the optical study of II–VI NPs obtained by means of colloidal chemistry under comparatively mild conditions from aqueous solutions stabilized by organic polymers (polyvinyl alcohol, gelatin, polyethyleneimine). The NPs have been characterized by optical absorption, photoluminescence, and Raman scattering spectroscopy. This report is a compact review of our original results obtained during the last several years. The following problems are discussed: a) spectroscopic evidences of size effects in the electron and phonon spectra of polymer-stabilized CdS and CdSe NPs; b) the effects of NP passivation by a wider- or narrower-bandgap semiconductor material; c) the optical peculiarities of ultra-small (of diameter $d < 2$ nm) NPs, where a major part of NP are the surface atoms.

2. Experimental Details

The NPs studied in this work were synthesized in aqueous solutions, with the use of polyvinyl alcohol, gelatin, or polyethyleneimine as a stabilizer. The synthesis of CdS and CdSe NPs occurred during the reaction between $CdCl_2$ (or $CdSO_4$) and Na_2S (or Na_2SeSO_3). The details of the synthesis have been published elsewhere [19, 20]. Methods of surface passivation are described, for example, in [20, 21]. For optical measurements, NP-containing films were prepared by drying the solvent from a colloidal solution deposited onto the glass plates at room temperature for several days. Absorption spectra of the films were recorded using a Specord 220 or HP Agilent 8453 spectrophotometer. Photoluminescence (PL) and Raman scattering spectra were recorded, by using Dilor XY 800, DFS-24 (LOMO), or Jobin Yvon T 64000 spectrophotometers. The PL spectra were excited with a 441.7-nm line of a He-Cd laser. All Raman spectra were unpolarized and recorded in the back-scattering geometry, by using various wavelengths of Ar^+ and He-Cd
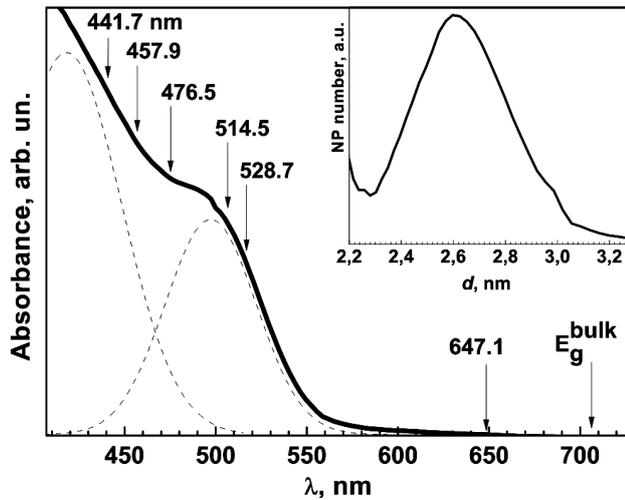
Fig. 1. A representative optical absorption spectrum of gelatin-embedded CdSe NPs under study. A fit to the first two absorption maxima is shown by the dashed line. Inset: size dispersion derived from the absorption spectrum based on the procedure developed in Ref. [22]

Fig. 2. Representative absorption and PL spectra of CdSe NPs stabilized with gelatin

lasers. The resolutions in the PL and Raman spectra were better than 1 nm and 3 cm^{-1}, respectively.

3. Size Effects on Optical Spectra of CdS and CdSe NPs in Polymer Films

3.1. Optical absorption and photoluminescence

Figure 1 shows a typical optical absorption spectrum of gelatin-embedded CdSe NPs of diameters as small as 2.7 nm. A large shift of the absorption edge of NPs from that of a bulk CdSe crystal evidences the strong spatial confinement of charge carriers in NPs. By arrows, we show the spectral positions of the laser wavelengths used for the excitation of resonant Raman spectra. The lowest absorption feature near 500 nm (schematically shown by a dashed Gaussian profile) corresponds to the lowest electronic transition $1S_e1S_{3/2}$ (HOMO–LUMO). The energy position of this absorption feature allows the average size $\bar{d}$ and the size distribution Δd of NPs to be estimated (inset to Fig. 1) by using the following relation derived in [22]: $n(r) \sim \frac{dA/dr}{(4/3)\pi r^3}$. Here, the absorbance A is given by $A(r) \sim \int_r^\infty 4/3\pi r^3 n(r)dr$. Note that we modified the model from [22] by substituting the size dependence of the NP bandgap, $E_g(d)$, based on the effective mass model, by a phenomenological one [23] which shows a much better agreement with experiment in the range of small d studied here. The latter dependence [23] was built based on the thorough study
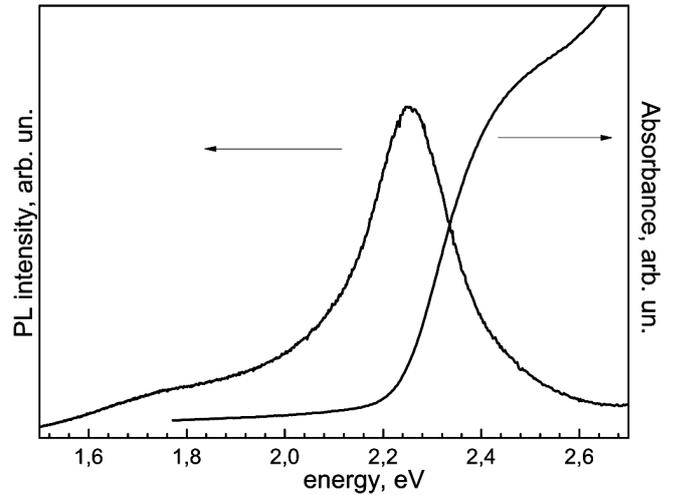
of numerous NP samples by transmission electron microscopy (TEM) and showed a good agreement with the data of other authors, while the commonly used effective mass approximation (EMA) [24] results in a considerable deviation from the experimental data for small nanoparticles ($d < 3$ nm) [23]. A potential-morphing method for nanoparticle size evaluation from the absorption spectra, based on the EMA [25], is not quite convincing, since the choice of the confinement potential for charge carriers in CdS nanoparticles, depending on the host matrix bandgap energy, does not seem to be justified. By comparing the results of [24] and [25] with each other and with the experimental data, one can see that the effect of the confinement potential (i.e., of the host matrix, as follows from [25]) is revealed only for NPs with $d < 3$ nm.

The PL spectra of CdSe NPs (Fig. 2) reveal at least two components. A near-bandgap emission peak at around 2.25 eV is often explained in the "dark exciton" model with regard for the exciton state fine structure due to the structural anisotropy and the electron-hole exchange interaction [24]. An alternative explanation, especially regarding the PL band width, is based on the exciton–acoustic phonon scattering [25]. The Stokes shift (the energy difference between the first absorption maximum and the near-bandgap emission peak) in gelatin-embedded CdSe nanoparticles is rather large – ~ 200 meV. According to the model in [26], the magnitude of ΔS increases with a decrease of the mean NP size and with an increase of the size dispersion. The dependence $\Delta S(d)$ becomes extremely steep for d below 3 nm and could evidently reach values close to 200 meV
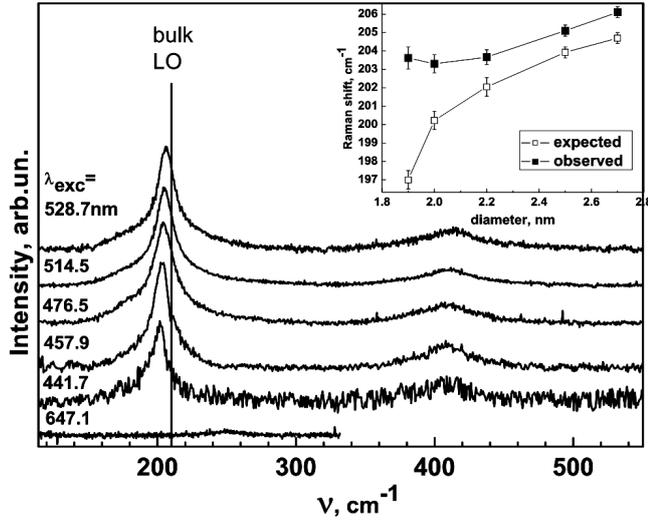
Fig. 3. Resonant Raman spectra of CdSe NPs in the region of the LO and 2LO phonon bands at different λ_{exc} noted over the absorption spectrum in Fig. 1. The vertical line shows the position of the LO peak for bulk CdSe. Inset: LO band maximum derived from the experimental spectra in comparison with the prediction of the phonon confinement model (see [30])

for the present NPs with a mean size of 2.8–2.9 nm and a size dispersion of 15–20% [19, 20].

A broader band, significantly shifted toward lower energies (~ 1.8 eV), is attributed to the recombination mediated by surface states, in particular anion vacancies [14, 15, 27–29]. Its weak spectral dependence on the nanoparticle size, as well as a noticeable suppression after the surface passivation (discussed in Section 4), is consistent with its assignment to sulfur vacancies located on the NP surface [6, 28].

3.2. Raman scattering

We have investigated the size effects on Raman spectra of CdS [21, 29] and CdSe [30] NPs in different polymers. Since NPs comprise only a small fraction (of the order of 1%) of the sample scattering volume, resonant conditions are required in order to obtain a sufficient Raman signal. For a given excitation laser wavelength, the average Raman cross-section per unit solid angle Ω_s and unit frequency ω_s of the NPs with a certain size distribution is given by [31]

$$\left\langle \frac{d^2\sigma}{d\omega_s d\Omega_s} \right\rangle = \int \frac{d^2\sigma}{d\omega_s d\Omega_s}(R)F(R)dR, \qquad (1)$$

where $F(R)$ is the distribution function of nanoparticles over radii R. According to the function $F(R)$, the resonant conditions select NPs with radii $\{R_i\}$ for the Ra-

man spectra [30]. These particular NPs give the main contribution to the spectrum selecting those phonon modes with frequencies $\omega_{n_p}(n_p = 0, R_i)$ (the modes are labeled by a set of integer numbers $p \equiv [n_p, l_p, m_p]$ where l_p and m_p are related to their symmetry properties and angular momentum). Hence, an asymmetric and broadened Raman lineshape is obtained due to several optical vibrations with different quantum numbers n_p participating in the process. The relative contribution of the confined phonon and excitonic states to the cross-section depends on the exciting laser energy, the excitonic oscillator strength, and the electron-phonon Fröhlich interaction. In particular, when the incoming or scattered light selects nanoparticles with small radii, the phonon line shape will be more asymmetric. For a given phonon mode in a NP with radius R, the frequency uncertainty $\delta\omega_{n_p}$ can be evaluated as [31]

$$\frac{\delta\omega_{n_p}}{\omega_{n_p}} = \frac{(\beta_L \mu_n)^2}{(\omega_{LO}R)^2 - (\beta_L \mu_n)^2}\frac{\delta R}{R}, \qquad (2)$$

where β_L is a parameter characterizing the bulk LO phonon dispersion, ω_{LO} is the LO phonon frequency, μ_n is the n-th zero of the spherical Bessel function j_1, and $\delta R \geq |R - R_i|$. Hence, the greater contribution to the resonant Raman spectrum will be made by those NPs of the ensemble, for which the excitonic transition energy coincides with the energy of the exciting (incoming resonance) or scattered (outgoing resonance) light. Therefore, in order to trace the size-dependent shift of the LO phonon frequency in NPs, resonant Raman measurements at a series of excitation wavelengths are required.

We have studied the dependence of Raman spectra on excitation wavelengths for CdSe NPs embedded in gelatin (Fig. 3) [30].

The first observation easy to make from Fig. 3 is that the LO peak maximum for all the λ_{exc} is by several wavenumbers lower than that of bulk CdSe (indicated by a vertical line). This shift is the indication of the phonon confinement (PC) effect [32–35]. A simple way to consider the PC effect on the phonon spectra of NPs was proposed by Richter [34] within a simple spatial correlation model, being in use till now with some modifications [35]. Later, a rigorous continuum theory [36, 37] and microscopic lattice dynamics calculations were applied considering discrete confined optical vibrational modes (vibrons), with the dominant contribution to the resonant Raman spectrum of the modes with quantum numbers $l_p = 0$ and 2 and $n = 1$ and 2 [31]. Any PC model employs the phonon dispersion of the bulk material to

predict the ν_{LO} in NPs. As the experimental dispersions, usually obtained by neutron scattering, are lacking for CdSe due to a large capture cross-section of neutrons in this material, only theoretical curves are available. This fact, along with a certain freedom in choosing the confinement function in the spatial correlation model [34], may be among the main reasons for a deviation between $\nu_{LO}(d)$ dependences obtained by the PC model and between this model and experiment (Fig. 3).

In Fig. 3, we see that the position of the LO peak for present CdSe NPs varies slightly with λ_{exc}. Considering the dispersion of the NP size of about 15% in our samples and the dependence of the LO phonon frequency (ν_{LO}) on the NP diameter d due to the PC effect, we can conclude that, by changing λ_{exc}, we selectively excite NPs of different average sizes [30].

Along with the downward shift of the phonon peak, the PC model predicts the broadening of the peak with probing smaller NPs. Instead, we observe a slight non-monotonic variation of the fundamental peak width, Γ_{LO}, between the different λ_{exc}. We suppose that the variation of Γ_{LO} is a result of the interplay between the PC, structural disorder, and width of the "resonant" region of the NP diameters [36]. We consider the size selectivity of the Raman scattering under the resonant excitation as one of the reasons for the scatter of the experimental data on the ν_{LO} dependence on NP size in the literature, as discussed in our work [30] in detail. Based on the above discussion, different conclusions about the magnitude of PC and strain in NPs can be obtained for the same NP sample, depending on λ_{exc} employed. In the opposite case where the same λ_{exc} is applied to NP ensembles with different mean d but overlapping size distribution profiles, the preferential selection of the NPs with the same d, favorable for this λ_{exc}, can lead to the observation of the same spectrum for both samples [30].

Let us now return to the present λ_{exc} dependence of ν_{LO} Fig. 3. The decrease of ν_{LO} for λ_{exc} varied from 528.7 down to 457.9 nm is in accordance with the selection of smaller NPs with shorter λ_{exc}, because smaller NPs possess a larger bandgap due to a stronger confinement of charge carriers and smaller ν_{LO} due to a stronger phonon confinement and the negative dispersion of LO phonons in CdSe [30]. The shortest wavelength excitations of 457.9 and 441.7 nm do not follow the downward shift of ν_{LO} predicted by the PC model and observed for longer λ_{exc}. Two possible explanations of this observation can be assumed. The first one is a size-dependent stress (larger for smaller NPs) observed for NPs in glasses [38]. We studied the possible strain effect of the gelatin matrix by measuring the spectra of
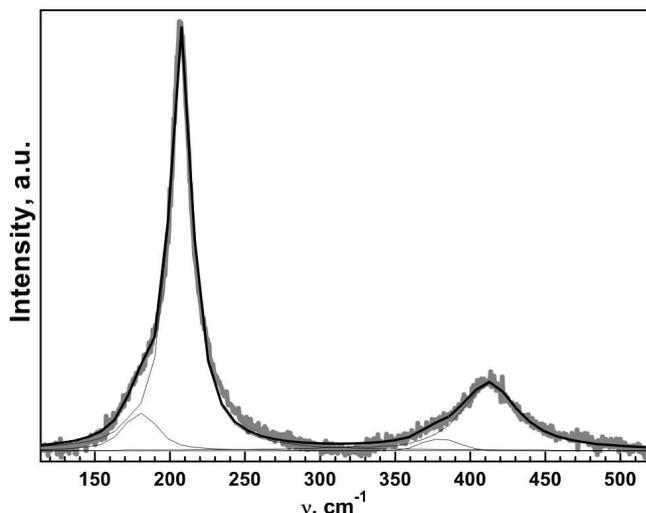

Fig. 4. Fitting of the LO and 2LO Raman bands with two Lorenzian profiles

the same NPs in the colloidal solution and in the rigid polymer matrix and detected no significant (beyond the experimental error) deviation neither of ν_{LO} nor of Γ_{LO}, indicating that no additional strain arises after embedding NPs into the polymer film.

All the spectra from the present NPs reveal a low-frequency shoulder (asymmetry) of the main LO peak, which has also been observed for a wide range of semiconductor NPs and assigned to a confinement-induced scattering by LO phonons with nonzero angular momenta [34] and/or to a contribution from surface optical (SO) phonon modes [33]. The importance of the surface for the NPs under study is obvious, as the portion of the surface atoms for NP of about 3 nm in diameter is about 50%. The theory accounting for the Raman scattering on confined optical vibrations (vibrons) allows only vibrons with zero angular momentum ($l_p = 0$) and the quantum number $n = 0$ in this process [36, 37]. Such factors as a non-sphericity of NPs and the hole sub-band mixing relax the $n = 0$ selection rule, and vibrons with $n = 2$ may be allowed, including the so-called surface-like modes [37]. It can be seen from Fig. 4 that the RRS spectrum in the range of LO and 2LO bands can be satisfactorily fitted with two Lorentzians, tentatively ascribed to the LO and SO modes, respectively, in accordance with results in [33, 38]. Only in particular cases of low-temperature Raman spectra of quasimonodisperse NP samples, additional weaker modes can be resolved, attributed to TO vibrations and, probably, some higher-order modes or surface-related vibrations (molecular Se, for example, or its oxide) [39, 40]. Within the dielectric

continuum model, for nanospheres with diameter d embedded in a medium with a real frequency-independent dielectric constant ϵ_m, surface-related modes should be observed at the frequencies $\omega_{\mathrm{SO},l}$ between those for LO and TO phonons of the nanosphere material ω_{TO} and ω_{LO}, corresponding to [33]

$$\epsilon_\infty \left[1 + \frac{\omega_{\mathrm{LO}}^2 - \omega_{\mathrm{TO}}^2}{\omega_{\mathrm{TO}}^2 - \omega_{\mathrm{SO}}^2} \right] = \frac{l+1}{l}\, \epsilon_m, \qquad (3)$$

where $l = 1, 2, 3, \ldots$ The intensity of these modes in nanoparticles decays with increase in the distance to the sphere surface as $1/r^{l-1}$ except for the so-called Fröhlich mode for $l = 1$ which has constant amplitude over the whole volume of the sphere [33]. Evidently, the contribution of the surface phonons to the Raman spectrum becomes increasingly important with increase in the surface-to-volume ratio. Being considerably broader than the LO phonon bands, surface phonons in nanoparticles are usually not observed as separate spectral maxima, but rather as a shoulder or the asymmetry at the low-frequency side of the LO phonon peak.

4. Investigation of Core–Shell Nanoparticles

4.1. Optical absorption and photoluminescence

In semiconductor NPs and other nano-sized systems with the number of the surface atoms comparable to that of the inner ones, the surface plays a crucial role in determining the physical properties of the structures and their applications [1]. As the surface atoms act as defect states, by trapping charge carriers and by deteriorating the emission properties of NPs, a number of passivation procedures have been developed in order to diminish their negative effect [42]. Organic ligands cannot passivate both cationic and anionic surface traps simultaneously [42]. Particles passivated by a layer of a wider-bandgap semiconductor material – "core–shell" NPs – are more robust than organic-passivated nanoparticles and therefore have a greater tolerance with respect to the processing conditions necessary for the incorporation into functional structures [42]. In this case, the non-radiative decay channels through surface states are not accessible for electrons confined inside the core. Therefore, such core-shell structures show a higher photoluminescence (PL) quantum yield [5, 20, 41, 42].

Significant progress has already been achieved in the synthesis of CdSe NPs passivated with a single layer of sulfide or selenide using, e.g., CdS, ZnS, ZnSe [42]. In our case, a solution of $CdSO_4$ or $Zn(NO_3)_2$ was added to the gelatin-stabilized CdSe colloids to form the shell

[20]. The colloids were kept under intense stirring for 5–10 min and then an amount of sodium sulfide equimolar to metal ions was added dropwise. The passivation was performed at several core-to-shell volumes and two ways of passivation: with the Cd(Zn)-supplying reagent being added before the sulfur-containing one ("Cd(Zn) – then S" scheme) and vice versa ("S – then Cd(Zn)") [43–46].

While the internal structure of homogeneous NPs can be studied by high-resolution transmission electron microscopy (HRTEM) [1, 23], the internal structure of the shell and the interface between a core and a shell are hardly discernible. X-ray diffraction (XRD) analysis shows a clear contribution from, e.g., the ZnS shell only for samples with a high ZnS coverage, because the scattering factors of ZnS are smaller than those of CdSe. At the same time, the potential of resonant Raman scattering (RRS) in exploring the structure of even sub-monolayer-thick heteronanostructures has recently been demonstrated [47–49] and employed in our investigations of the core-shell NPs [43–46]. The main results obtained are summarized below.

1. Passivation of the NP with a layer of larger-bandgap semiconductor results in a shift of their absorption and PL to longer wavelengths. The shift has been observed for different core-shell materials and explained by the partial tunnelling of the electron wave function into the shell. The magnitude of the shift increases with the shell thickness or, in the case of equally thick shells, for the shell made of a lower band-gap material [20, 42].

2. The effect of the shell formation on the PL spectra is revealed also in an increase in the intensity of the near-bandgap emission by a factor up to 5 [20]. This effect is sensitive to the volume of the passivating material. After reaching a certain critical shell thickness, the PL intensity decreases due to the formation of dislocations in the shell [42].

Another important factor is which sort of atoms is added first: metal or sulfur. For the same volume of the shell-forming reagents (1:1) in the case "Cd then S," a much higher PL intensity is achieved than that in the case where the scheme "S then Cd" is applied (Fig. 5), while the shifts of the absorption and emission maxima are very close in both cases. From these results and a number of other studies [41, 42], it follows that there exists an optimal, in view of the light emission properties, thickness of the shell, which is different for every particular method of NP preparation and passivation. The "right" reagent addition sequence seems to be even more important in the case of the ZnS shell. Thus, the "Zn then S" addition scheme gives a PL increase by a factor of 5, while the opposite sequence quenches the PL by a

factor of 3. The latter fact may also be a consequence of the existence of the optimal thickness for every passivation scheme (sequence of reagents), as in the above case of CdS shells.

3. In the Raman spectra of the NPs passivated with CdS, an additional peak at 280 cm^{-1} is observed as compared to bare CdSe NPs (Fig. 6). As the frequency of Raman-active LO phonons in bulk CdS is 305 cm^{-1} [50] and decreases down to 280–300 cm^{-1} in thin layers and superlattices [51], the observed peak can be attributed to LO phonons in the CdS shell. Such downward shift from the bulk LO phonon frequency can result from the phonon confinement and a strain. However, since the shift is fairly large, one can hardly attribute it solely to confinement effects, for which a shift less than about 5 cm^{-1} could be expected based on the experimental results for thin epitaxial CdS layers [51]. The significant broadening of the peak can be a result of the phonon confinement and the inhomogeneity of the very thin passivating layer.

The Raman spectrum of the sample with a higher thickness of the CdS shell ([CdSe]:[CdS] = 1:3) differs from that with [CdSe]:[CdS] = 1:1 (at the same passivation scheme "S then Cd") with a higher frequency and a higher intensity of the CdS-like peak (Fig. 6). Both the absorption and PL bands of this sample show larger "red" shifts with respect to the unpassivated CdSe NPs spectrum, as compared with the case of [CdSe]:[CdS] = 1:1, evidently indicating an increase of the thickness of the passivating layer. But the growth of the CdS-like peak intensity in the case of CdSe/CdS NPs is unlikely to be directly related to the augmentation of the scattering (shell) volume. We relate it to a decrease of the energy of the resonant electronic transition in the shell, as its thickness increases, resulting in a better matching of the resonant conditions.

The importance of resonant conditions for the observation of this peak should be noted. The increase of both the intensity and the width of the CdS-like peak at shorter excitation wavelengths λ_{exc} (Fig. 7) can be a result of the inhomogeneity of the shell thickness among the NPs.

More intriguing were results for CdSe NPs passivated with ZnS. The typical Raman spectra for such structures are shown in Fig. 8. The shell-induced Raman peak observed for CdSe/ZnS NPs at almost the same frequency, 280 cm^{-1}, as that of a CdS-like phonon in CdSe/CdS NPs, was quite surprising. Indeed, the calculation of the LO phonon frequency for a thin ZnS layer grown coherently on a CdSe substrate gives a value of about 300 cm^{-1}. The downward shift by 50 cm^{-1} with re-
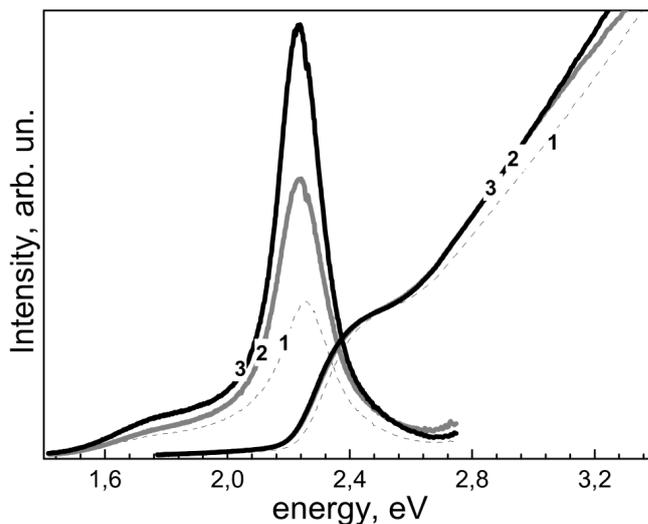

Fig. 5. Absorption and PL spectra of CdSe NPs (1) and CdSe/CdS NPs passivated according to the "Cd – then S" (2) and "S – then Cd" (3) schemes with the final ratio of [CdSe]:[CdS] = 1:1 in both cases

spect to the bulk phonon frequency is due to the tensile strain induced by a lattice mismatch of 11% between CdSe and ZnS [51]. However, in the case of the growth on spherical NPs, the ZnS lattice has more freedom to relax the strain than in the two-dimensional case and therefore cannot reach the frequency we observe – 280 cm^{-1}. Therefore we cannot relate the observed feature at 280 cm^{-1} with the LO phonon of the ZnS shell. We believe that it is more reasonable to relate this band with Cd–S-like vibrations in the alloyed interface layer of the $Cd_yZn_{1-y}Se_xS_{1-x}$ composition, in the general case, which is formed as a result of the compositional intermixing (interdiffusion) during the formation of the shell.

5. Synthesis and Optical Properties of Ultrasmall White-Light Emitting CdS, CdSe, and CdS_xSe_{1-x} NPs

Ultrasmall semiconductor nanoparticles or quantum dots, with a diameter less than 2 nm, have become a recent topic of intense investigations [6, 7]. First of all, the interest is driven by their inherent broad photoluminescence (PL) spectrum, promising for applications in the white-light emitting devices. Furthermore, the nanoparticles of such small size are attractive as luminescent markers for those bio- and medical applications where the nanoparticle size is a critical parameter concerning the penetration of functionalized NPs through the cell walls.
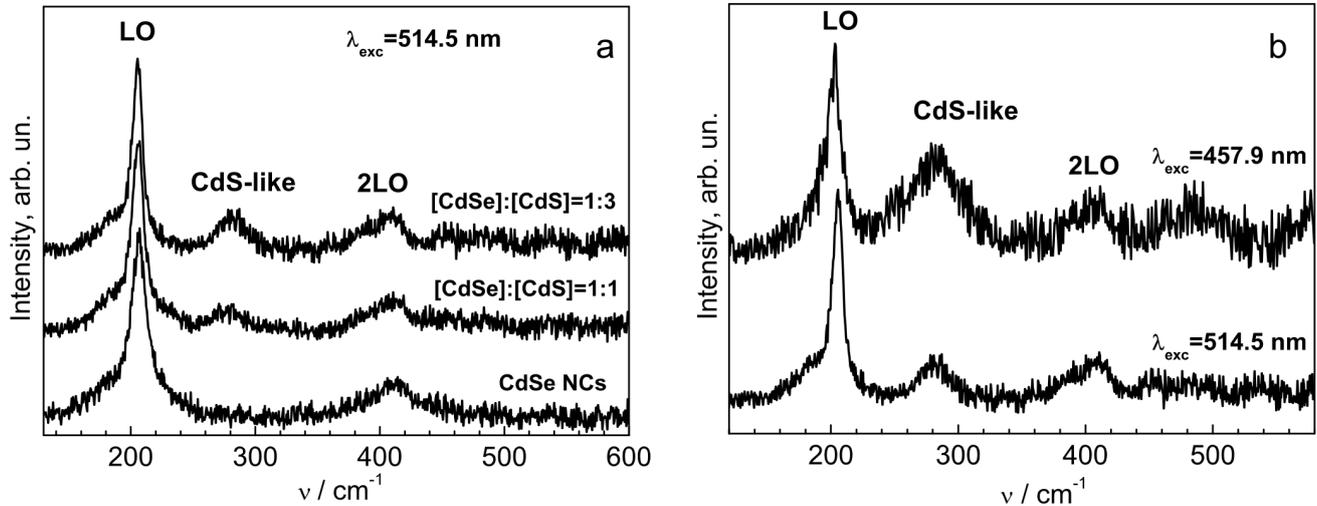
Fig. 6. (*a*) Resonant Raman scattering spectra of CdSe and CdSe/CdS ("S – then Cd" scheme) NPs for various shell thicknesses. Raman spectra of CdSe/CdS NPs at various λ_{exc}
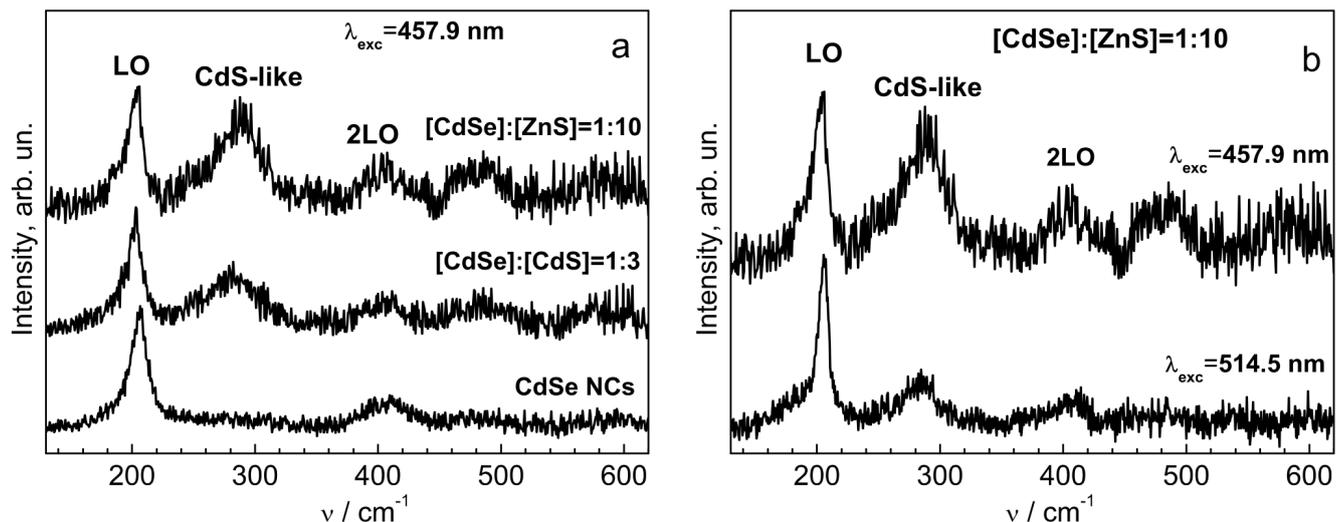

Fig. 7. (*a*) Resonant Raman scattering spectra of CdSe and CdSe/ZnS ("S – then Cd" scheme) NPs of for various shell thicknesses. (*b*) Raman spectra CdSe/ZnS NPs at various λ_{exc}

The conjugation of NPs with bio-friendly polymers in the process of NP synthesis is of particular significance, as it allows one to avoid the loss of the PL intensity at the stage of ligand exchange and transfer from organic to aqueous media [1]. Recently, we have reported on the synthesis and the characterization of ultrasmall (< 2 nm) CdS, CdSe and mixed CdS_xSe_{1-x} NPs prepared in aqueous and alcohol solutions of polyethyleneimine [52–54]. Polyethyleneimine (PEI) is known to be a polyelectrolyte applicable in the fabrication of thin-film NP-based light-emitting devices, as well as an effective transfection agent

in the intracellular DNA and the delivery of genes [55].

In this work, the highly luminescent (with the quantum yields up to 30% at room temperature) CdS_xSe_{1-x} NPs with a broad (white-like) emission have been synthesized directly in the solution of PEI used as both the stabilizing and surface-passivating agent. The details of the synthesis can be found elsewhere [52–54]. In opposite to other kinds of colloidal II–VI NPs synthesized before with the use of bio-compatible polymers as a stabilizer, the PEI-stabilized NPs manifest the PL quantum yield (up to 30%) and the concentration of colloidal particles
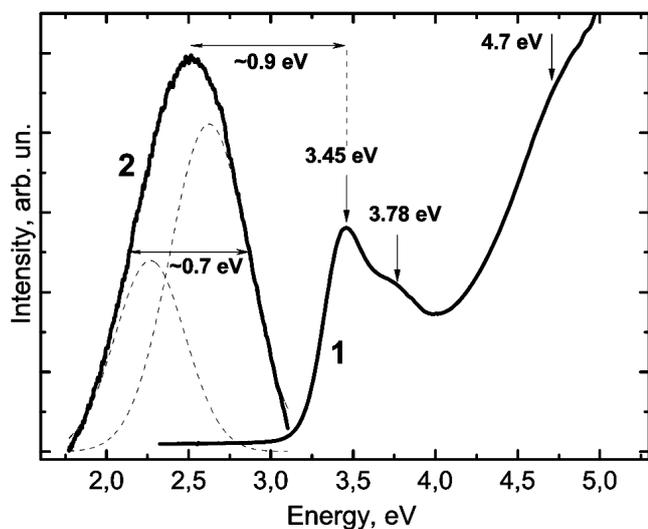
Fig. 8. Normalized typical absorbance (curve *1*) and PL (*2*) spectra of colloidal PEI-stabilized CdS NPs in water. Dash lines: a two-Gaussian deconvolution of the PL spectrum

Fig. 9. Optical absorption spectra of CdS_xSe_{1-x}-PEI NPs under study

(up to 50% of the polymer mass), at the smallest possible size dispersion – 3–5%.

In the optical absorbance spectra of PEI-stabilized CdS NPs (Fig. 8), two distinct features are observed, E_1 at 3.45 eV and E_2 at 3.78 eV, shifted to higher energies by about 1.0 eV as compared to those in bulk CdS. These features can be assigned to the $1S_e$–$1S_{3/2}$ and $1S_e$–$2S_{3/2}$ interband transitions, respectively [26]. The third feature at about 4.7 eV is also visible. The average size of PEI-stabilized CdS NPs reported here was estimated, based on the E_1 peak position in the absorbance spectra (Fig. 1) [54], as $d = 1.8 \pm 0.1$. The spectral width (FWHM) of E_1 peak, $\Gamma_{E_1} = 0.3$ eV corresponds to a size distribution of $\sim 10\%$.

On the basis of X-ray patterns of PEI-stabilized CdS NPs reported in [54], we could only conclude that they are rather crystalline than amorphous. But, due to the large width of the peaks, it was not possible to distinguish between zinc-blend and wurtzite structures.

The optical absorption spectra of CdS_xSe_{1-x} NPs under study (Fig. 9) reveal a smooth shift of the excitonic peaks between those of pure CdS and CdSe NPs, with their diameter d being almost unchanged, 1.8 ± 0.1 nm. The observed E_1 peak energies and the pronounced stability of this particular NP size, even at a noticeable variation of synthesis parameters, allowed us to attribute our NPs to the sort of magic-size NPs (MSNCs) reported by others [7]. Furthermore, the vibrational Raman band of the NPs under study is very similar to that of the
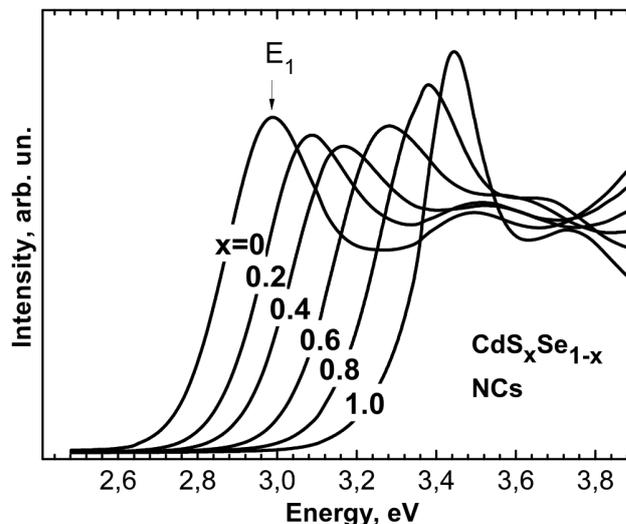
CdSe NPs studied in Ref. [7], the latter NCs being the magic-size ones undoubtedly (Cd_32Se_32).

The Raman spectra of the MSNCs under study (Fig. 10) reveal the main band centered well below the regularly most intense Raman-active longitudinal optical (LO) mode and close to the frequency of the surface optical (SO) mode reported as the low-frequency wing of the LO peak [30, 33, 37, 40]. The x-dependence of the SO frequency is very weak (due to opposite trends of LO and TO bands), similarly to that of Raman bands in Fig. 10. The Raman bandwidth of CdS_xSe_{1-x}-PEI NPs – 50 cm^{-1} – is also closer to that of the SO mode – 30–60 cm^{-1} [33], than of the LO one – commonly 10–15 cm^{-1} and not exceeding 30 cm^{-1} [40, 41]. The dominance of the SO mode in present 1.8 nm NPs with the surface-to-volume atom ratio close to 1 appears rather reasonable. However, in the previous study of CdSe NPs in the d range from 4 down to 2 nm [40], we did not observed a trend of the dominance of the SO mode with decrease in the NP size, with an almost constant intensity ratio of ISO/ILO in the above size range, which magnitude also correlates with the data for larger NPs [30]. Thus, a dramatic change of the ISO/ILO ratio in present 1.8 nm NPs may evidence that their structure is different from that of NPs studied previously. The attempts to measure the size and the shape of a single MSNC directly by electron microscopy were unsuccessful [54], obviously due to the ultrasmall NP size and the charging of the stabilizing polymer under the action of an electron beam. The broad X-ray features for our MSNCs resembled those of amorphous semiconductors. In opposite,
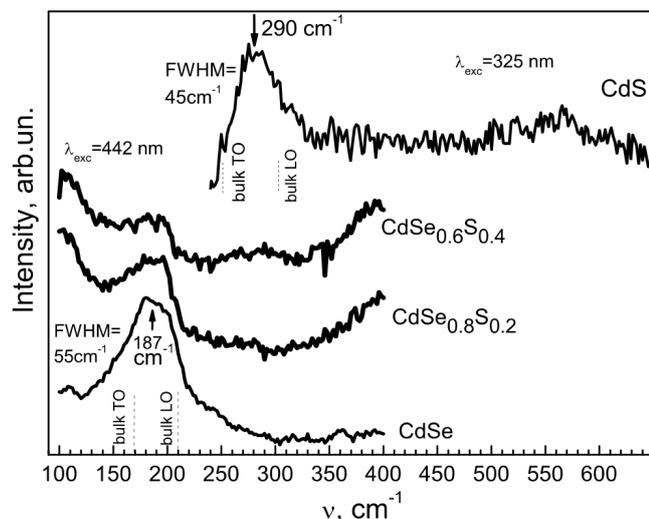
Fig. 10. Raman scattering spectra of CdS_xSe_{1-x} NPs under the resonant excitation with 325- or 442-nm laser lines [58]

the weak broad feature at 550–600 cm^{-1} in the spectrum of CdS-PEI NPs (Fig. 10) can be assigned to the LO overtone which is common for crystalline II–VI semiconductors [14, 24]. Though, the MSNCs may preserve, in general, the structure of the corresponding bulk crystal, the size of 2 nm may turn to be a critical one for propagating lattice vibrational modes (phonons), and smaller NPs may not support the long-wavelength LO mode. The domination of under-coordinated atoms in 1.8-nm NPs can cause the phonon density of states (DOS) to be revealed in the Raman spectra, as in the case of amorphous or strongly disordered semiconductors. The similarity of the phonon spectra in MSNC and an amorphous material can be due to that the MSNC size is close to the short-range order distance in the amorphous state – ~ 2 nm for II–VI compounds under study. The Raman band of present CdSe MSNCs is indeed close to the phonon DOS profile calculated for CdSe nanowires with $d = 2$ nm [56]. The reduction of the TO–LO splitting in ultra-small clusters, proposed in Ref. [57], can also contribute to the broadening and the downward shift of the phonon band.

In addition to the above-discussed effects, the distortion of bond lengths and angles due to the minimization of the NP energy and a noticeable change of the elastic properties can also contribute to both the frequency shift and the broadening of the vibrational Raman peak [58]. Raman measurements performed on CdS_xSe_{1-x} NPs of about twice larger size, obtained by their ripening at room temperature, revealed much narrower Raman peaks [59]. The latter fact also indicates that the

initially large Raman band width is related to the small NP size (< 2 nm), rather than to their poor crystallinity.

6. Conclusion

In conclusion, semiconductor nanoparticles and core–shell nanoparticles based on II–VI semiconductor compounds have been prepared and studied by means of optical absorption, photoluminescence, and Raman scattering spectroscopy. The effects of the strong confinement of charge carriers and lattice vibrations in these small (< 3 nm) semiconductor nanoparticles have been observed. The noticeable influence of the passivating shell onto the optical bandgap, spectral position, and intensity of photoluminescence has been found. The appearance of a new feature in the Raman phonon spectrum of core–shell NPs is related to the compositional intermixing at the core-shell interface. The drastic difference in resonant Raman spectra of ultra-small (< 2 nm) nanoparticles is referred to both the strong spatial localization of vibrations in NPs and their structural rearrangement due to the surface effect.

1. *Semiconductor Nanocrystal Quantum Dots: Synthesis, Assembly, Spectroscopy and Applications*, edited by A. Rogach (Springer, New York, 2008).

2. Q. Dai, C.E. Duty, and M.Z. Hu, Small **6**, 1577 (2010).

3. A. Fahmi, T. Pietsch, D. Appelhans, N. Gindy, and B. Voit, New J. of Chemistry **33**, 703 (2009).

4. A.M. Kelley J. Phys. Chem. Lett. **1**, 1296 (2010).

5. F. Garcia-Santamaria, S. Brovelli, R. Viswanatha, J.A. Hollingsworth, H. Htoon, S.A. Crooker, and V.I. Klimov, Nano Lett. **11**, 687 (2011).

6. S.A. Gallagher, M.P. Moloney, M. Wojdyla, S.J. Quinn, J.M. Kelly, and Y.K. Gun'ko, J. Mater. Chem. **20**, 8350 (2010).

7. Y.-S. Park, A. Dmytruk, I. Dmitruk, A. Kasuya, M. Takeda, N. Ohuchi, Y. Okamoto, N. Kaji, M. Tokeshi, and Y. Baba, ACS Nano **4**, 121 (2010).

8. N. Radychev, I. Lokteva, F. Witt, J. Kolny-Olesiak, H. Borchert, and J. Parisi, J. Phys. Chem. C **115**, 14111 (2011).

9. E. Zenkevich, F. Cichos, A. Shulga, E.P. Petrov, T. Blaudeck, and C. von Borczyskowski, J. Phys. Chem. B **109**, 8679 (2005).

10. E.-J. Park, T. Erdem, V. Ibrahimova, S. Nizamoglu, H.V. Demir, and D. Tuncel, ACS Nano **5**, 2483 (2011).

11. N.E. Korsunska, M. Dybiec, L. Zhukov, S. Ostapenko and T. Zhukov, Semicond. Sci. Technol. **20**, 876 (2005).

12. V. Korbutyak, S.M. Kalytchuk, Yu.B. Khalavka, and L.P. Shcherbak, Ukr. J. Phys. **55**, 822 (2010).

13. F. Gaspari, I.M. Kupchak, A.I. Shkrebtii, and J.M. Perz, Phys. Rev. B **79**, 224203 (2009).

14. N.V. Bondar and M.S. Brodyn, Ukr. J. Phys. **54**, 130 (2009).

15. A.L. Stroyuk, A.I. Kryukov, S.Ya. Kuchmii, and V.D. Pokhodenko, Theor. and Experim. Chem. **41**, 67 (2005).

16. Ch.-S. Lim, M.-L. Chen, and W.-Ch. Oh, Korean Chem. Soc. **32**, 1 (2011).

17. M. Mozafari and F. Moztarzadeha, J. Colloid and Interf. Sci. **351**, 442 (2010).

18. Y. Wang, Ch. Ye, L. Wu, and Y. Hu, J. Pharm. and Biomed. Analysis **53**, 235 (2010).

19. A.E. Raevskaya, A.L. Stroyuk, S.Ya. Kuchmiy, Yu.M. Azhniuk, V.M. Dzhagan, V.O. Yukhymchuk, and M.Ya. Valakh, Colloids and Surfaces A: Physicochem. Eng. Aspects **290**, 304 (2006).

20. A.E. Raevskaya, A.L. Stroyuk, S.Ya. Kuchmii, V.M. Dzhagan, M.Ya. Valakh, D.R.T. Zahn, and S. Schulze, J. Phys.: Condensed Matter **19**, 386237 (2007).

21. V. Dzhagan, O. Rayevska, O. Stroyuk, S. Kuchmiy, and D.R.T. Zahn. Phys. Stat. Sol. (c) **6**, 2043 (2009).

22. N.S. Pesika, K.J. Stebe, and P.C. Searson, J. Phys. Chem. B **107**, 10412 (2003).

23. C. de Mello Donega and R. Koole, J. Phys. Chem. C **113**, 6511 (2009).

24. M. Nirmal, D.J. Norris, M. Kuno, M.G. Bawendi, Al.L. Efros, and M. Rosen, Phys. Rev. Lett. **75**, 3728 (1995).

25. S. Baskoutas and A.F. Terzis, J. Appl. Phys. **99**, 013708 (2006).

26. M. Kuno, J.K. Lee, B.O. Dabbousi, F.V. Mikulec, and M.G. Bawendi, J. Chem. Phys. B **106**, 9869 (2003).

27. O.L. Stroyuk, V.M. Dzhagan, V.V. Shvalagin, and S.Ya. Kuchmiy, J. Phys. Chem. C **114**, 220 (2010).

28. A.L. Stroyuk, V.M. Dzhagan, D.R.T. Zahn, and C. von Borczyskowski, Theor. and Experim. Chem. **43**, 297 (2007).

29. Yu.M. Azhniuk, V.M. Dzhagan, Yu.I. Hutych, A.E. Raevskaya, A.L. Stroyuk, S.Ya. Kuchmiy, M.Ya. Valakh, and D.R.T. Zahn, J. of Optoelectr. and Adv. Mater. **11**, 257 (2009).

30. V.M. Dzhagan, M.Ya. Valakh, A.E. Raevskaya, A.L. Stroyuk, S.Ya. Kuchmiy, and D.R.T. Zahn, Nanotechn. **19**, 305707 (2008).

31. C. Trallero-Giner, Phys. Stat. Sol. (b) **241**, 572 (2004).

32. D. Ristica, M. Ivanda, and K. Furica, J. Mol. Struct. **924-926**, 291 (2009).

33. A. Mlayah, A.M. Brugman, R. Carles, J.B. Renucci, M.Ya. Valakh and A.V. Pogorelov, Solid State Commun. **90**, 567 (1994).

34. H. Richter, Z.P. Wang, and L. Ley, Solid State Commun. **39**, 625 (1981).

35. G. Faraci, S. Gibilisco, A.R. Pennisi, and C. Faraci, J. Appl. Phys. **109**, 074311 (2011).

36. C. Trallero-Giner, A. Debernardi, M. Cardona, E. Menendez-Proupin, and A.I. Ekimov, Phys. Rev. B **57**, 4664 (1997).

37. A.G. Rolo and M.I. Vasilevskiy, J. Raman Spectrosc. **38**, 618 (2007).

38. E.S. Freitas Neto, S.W. da Silva, P.C. Morais, M.I. Vasilevskiy, M.A. Pereira-da-Silva, and N.O. Dantasa, J. Raman Spectrosc. DOI: 10.1002/jrs.2918 (2011).

39. V. Dzhagan, M.Ya. Valakh, J. Kolny-Olesiak, I. Lokteva, and D.R.T. Zahn, Appl. Phys. Lett. **94**, 243101 (2009).

40. V.M. Dzhagan, I. Lokteva, M.Ya. Valakh, O.E. Raevska, J. Kolny-Olesiak, and D.R.T. Zahn, J. Appl. Phys. **106**, 084318 (2009).

41. L. Lu, X.-L. Xu, W.-T. Liang, and H.-F. Lu, J. Phys. Condens. Matter **19**, 406221 (2007).

42. P. Reiss, M. Protiere, and L. Li, Small **5**, 154 (2009).

43. V.M. Dzhagan, M.Ya. Valakh, A.E. Raevskaya, A.L. Stroyuk, S.Ya. Kuchmiy, and D.R.T. Zahn, Nanotechn. **18**, 285701 (2007).

44. V.M. Dzhagan, M.Ya. Valakh, A.E. Raevskaya, A.L. Stroyuk, S.Ya. Kuchmiy, and D.R.T. Zahn, J. Phys. Conf. Series **92**, 012045 (2007).

45. V.M. Dzhagan, M.Ya. Valakh, A.E. Raevskaya, A.L. Stroyuk, S.Ya. Kuchmiy, and D.R.T. Zahn, Appl. Surf. Sci. **255**, 725 (2008).

46. V.M. Dzhagan, M.Ya. Valakh, O.E. Raevska, O.L. Stroyuk, S.Ya. Kuchmiy, and D.R.T. Zahn, Nanotechn. **20**, 365704 (2009).

47. A.G. Milekhin, A.I. Toropov, A.K. Bakarov, and D.A. Tenne, G. Zanelatto, J.C. Galzerani, S. Schulze, and D.R.T. Zahn, Phys. Rev. B **70**, 085314 (2004).

48. B.V. Kamenev, H. Grebel, L. Tsybeskov, T.I. Kamins, R.S. Williams, J.M. Baribeau, and D.J. Lockwood, Appl. Phys. Lett. **83**, 5035 (2003).

49. M.Ya. Valakh, R.Yu. Holiney, V.M. Dzhagan, Z.F. Krasil'nik, O.S. Lytvyn, D.N. Lobanov, A.G. Milekhin, A.I. Nikiforov, A.V. Novikov, O.P. Pchelyakov, and V.O. Yukhymchuk, Phys. Solid State **47**, 54 (2005).

50. T.T.K. Chi, G. Gouadec, Ph. Colomban, G. Wang, L. Mazerolles, and N.Q. Liem, J. Raman Spectrosc. **42**, 1007 (2011).

51. S. Zou and M.J. Weaver, J. Phys. Chem. B **103**, 2323 (1999).

52. A.E. Raevskaya, G.Ya. Grodzyuk, A.L. Stroyuk, S.Ya. Kuchmii, and V.N. Dzhagan, Theor. and Experim. Chem. **46**, 233 (2010).

53. A.E. Raevskaya, G.Ya. Grodzyuk, A.V. Korzhak, A.L. Stroyuk, S.Ya. Kuchmii, V.N. Dzhagan, M.Ya. Valakh, V.F. Plyusnin, V.P. Grivin, N.N. Mel'nik, T.N. Zavaritskaya, T.N. Kucherenko, and O.S. Plyashechnik, Theor. and Experim. Chem **46**, 416 (2011).

54. O.E. Rayevska, G.Ya. Grodzyuk, V.M. Dzhagan, O.L. Stroyuk, S.Ya. Kuchmiy, V.F. Plyusnin, and M.Ya. Valakh, J. Phys. Chem. C **114**, 22478 (2010).

55. A. Rogach, N. Gaponik, J.M. Lupton, C. Bertoni, D.E. Gallardo, S. Dunn, N. Li Pira, M. Paderi, P. Repetto, S.G. Romanov, C. O'Dwyer, C.M. Sotomayor Torres, and A. Eychmuller, Angew. Chem. Int. Ed. **47**, 6538 (2008).

56. M. Mohr and C. Thomsen, Nanotechn. **20**, 115707 (2009).

57. A.G. Rolo, M.I. Vasilevskiy, N.P. Gaponik, A.L. Rogach, and M.J.M. Gomes, Phys. Stat. Sol. (b) **229**, 433 (2002).

58. V. Dzhagan, N. Mel'nik, V. Strel'chuk, O. Plyashechnik, O. Rayevska, G. Grozdyuk, S. Kuchmii, and M. Valakh, Phys. Stat. Sol. RRL **5**, 250 (2011).

59. N.N. Melnik, T.N. Zavaritskaya, I.V. Kucherenko, O.S. Plyashechnik, M.Ya. Valakh, V.N. Dzhagan, and A.E. Raevskaya, Bulletin of the Lebedev Phys. Inst. **38**, 48 (2011).

ОПТИЧНІ ДОСЛІДЖЕННЯ НАДМАЛИХ КОЛОЇДНИХ НАНОЧАСТИНОК НАПІВПРОВІДНИКІВ A_2B_6 ТА ГЕТЕРОЧАСТИНОК НА ЇХ ОСНОВІ

М.Я. Валах, В.М. Джаган, О.Є. Раєвська, С.Я. Кучмій

Р е з ю м е

Наночастинки (НЧ) напівпровідників A_2B_6 та НЧ типу ядро–оболонка, отримані методом колоїдного синтезу, досліджено методами спектроскопії оптичного поглинання, фотолюмінесценції та комбінаційного розсіяння світла (КРС). Розглянуто ефекти сильного просторового обмеження носіїв заряду та коливань ґратки в НЧ малого розміру (> 3 нм). Встановлено вплив пасивуючої оболонки на ширину забороненої зони, спектр фотолюмінесценції та фононний спектр. Виявлено суттєві відмінності у коливному спектрі резонансного КРС надмалих (< 2 нм) НЧ, що пов'язується з сильним просторовим обмеженням коливних збуджень у цих НЧ та їх структурною перебудовою, зумовленою впливом поверхні.